ADVANCED FUNCTIONAL MATERIALS
www.afm-journal.de

Flexible and Robust 3D a-SiGe Radial Junction Near-Infrared Photodetectors for Rapid Sphygmic Signal Monitoring

Shaobo Zhang, Ting Zhang, Zongguang Liu, Junzhuan Wang, Jun Xu, Kunji Chen, and Linwei Yu**

Flexible near-infrared (NIR) photodetectors (PDs) are desired for accurate heart rate monitoring, based directly on arterial-blood-volume-change detection, instead of indirect oximetry technology. In this work, a robust 3D construction of flexible a-SiGe:H *p-i-n* radial junction (RJ) PDs is explored directly upon soft Al foils, working at NIR wavelength 800 nm, which has the highest skin transparency and the least absorption difference from oxyhemoglobin and deoxyhemoglobin variation. The 3D a-SiGe:H RJ-PDs demonstrate excellent flexibility and mechanical stability that can undergo 1000-times bending to 10 mm radius, with a high responsivity of ≈140 mA W^{-1}@800 nm and rise/fall time scales of 5.4 µs/17.6 µs (3.6 µs/13.2 µs before bending). Successful photoplethysmography (PPG) detection of sphygmic signals is achieved at the wrist with significant arterial blood volume changes, working in reflectance mode and using a single NIR source @800 nm. These unique capabilities, enabled by the a-SiGe:H RJ, have a promising potential to establish a reliable and convenient PPG detection technology, which can help to extract the heartbeat via solely arterial blood volume change, as a complementary and potentially very useful new diagnostic dimension for efficient and accurate real-time health monitoring.

1. Introduction

Flexible photodetectors (PDs) are attracting enormous research attentions for their widespread bio-sensing/detecting applications[1–7] in wearable and personalized medicine and real-time health monitoring.[8–12] Among all the physiological parameters, the heart rate is a vital physiological signal required for a wide range of diagnostics, which can be detected by using photoplethysmography (PPG) technique[13–17] easily but not accurately because there is significant movement artefact or cardiac arrhythmia in pulse oximetry PPG techniques that rely on the oxyhemoglobin and deoxyhemoglobin absorption difference for the red (≈625 nm) and green (≈530 nm) probing lights.[18] In order to directly measure the arterial blood volume change, which is considered as a more accurate reflection of the heart beating, near-infrared (NIR) probing light at ≈800 nm can be a better choice, as it can penetrate deeper into the human skin/tissue,[18–20] and more importantly, exclude the influence of oxyhemoglobin/ deoxyhemoglobin variation as their absorption difference almost disappear at this wavelength, as indicated in **Figure 1**a. On the other hand, the flexibility of the NIR PDs is another crucial feature required to achieve a bio-comfortable health monitoring attached closely to the soft human skin surface. To this end, 3D hydrogenated amorphous (a-Si:H) thin film radial junction (RJ) optoelectronic detectors, built over vertical Si nanowires (NWs) grown directly upon flexible aluminum (Al) substrates via vapor-liquid-solid (VLS) mechanism,[21] have several outstanding advantages. These include first a strongly enhanced light absorbing performance owing to the 3D architecture, which allows for the use of a very thin intrinsic absorber layer;[21–25] Second, the 3D RJ units can be directly grown upon soft Al foil (AF) substrates, where the standing SiNWs serve as firm anchor sites to host the active a-Si:H *p-i-n* junctions and protect them from the high-strain bottom surface. This unique feature enables an excellent flexibility and mechanical stability of the 3D RJ@AF devices, even under large bending, as well as a very high power-to-weight ratio performance.[21]

However, the a-Si:H RJ has a fundamental limit in terms of light absorption to NIR wavelength, due to its wider optical bandgap of ≈1.8 eV, corresponding to absorption up to 700 nm,[26] which cannot reach the targeted NIR wavelength working at 800 nm (see Figure 1b). A solution to address this challenge is to use hydrogenated amorphous silicon germanium (a-SiGe:H) alloy thin film, which can have a narrower band gap of $E_g \approx 1.4$ eV to extend the light absorption wavelength up to >880 nm, as verified in planar *p-i-n* junction devices.[27–30] Unfortunately, flexible a-SiGe:H RJ devices have never been explored to accomplish a direct PPG detection.

In this work, we demonstrated a rather flexible and robust construction of 3D a-SiGe:H RJ NIR PDs upon VLS-grown SiNWs directly grown on AF substrates of 50 µm thick, which can greatly extend the light detection wavelength from <700 nm to the NIR range, enabling thus a ultrafast sphygmic signal monitoring with outstanding flexibility. After 1000-times

S. Zhang, T. Zhang, Z. Liu, J. Wang, J. Xu, K. Chen, L. Yu
National Laboratory of Solid State Microstructures/School of Electronics Science and Engineering/Collaborative Innovation Center of Advanced Microstructures
Nanjing University
Nanjing 210093, P. R. China
E-mail: liuzongguang@nju.edu.cn; yulinwei@nju.edu.cn

The ORCID identification number(s) for the author(s) of this article can be found under https://doi.org/10.1002/adfm.202107040.

DOI: 10.1002/adfm.202107040

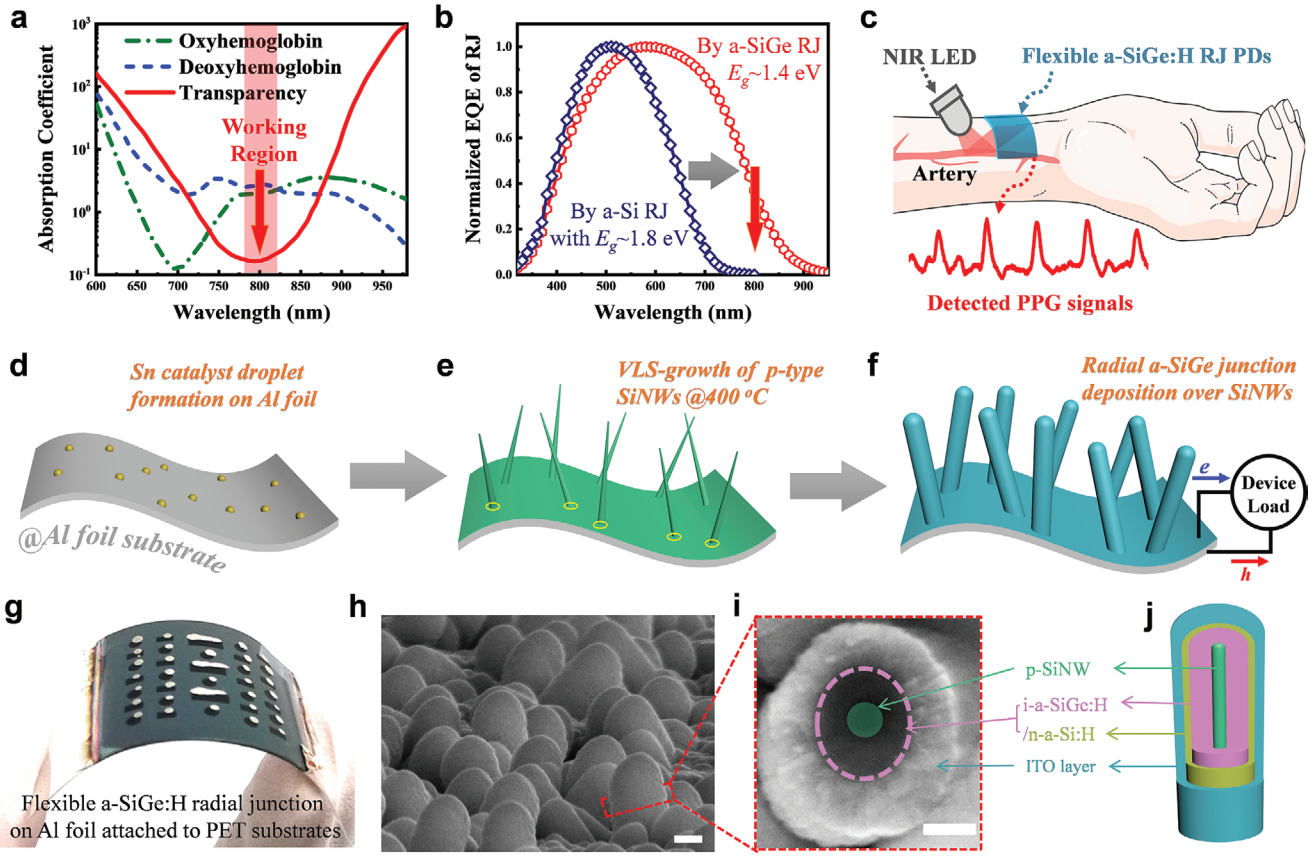

Figure 1. a) Indicative absorption coefficient curves of oxyhemoglobin and deoxyhemoglobin in human blood is shown in. b) Normalized EQE curves of the a-Si:H and a-SiGe:H RJs are presented in. c) Diagram of detecting pulse at wrist is shown in. Schematic illustrations of the fabrication procedure upon AF substrate: d) Sn catalyst formation by H_2 plasma treatment in PECVD system, followed by e) the VLS growth of p-type SiNWs, and f) the final-fabricated RJs with top ITO electrode layer. g) The photograph of flexible a-SiGe:H RJ NIR PDs attached to a bent PET substrate is shown in, and the h) side-view SEM image is presented. i,j) The SEM image of cross section and diagram of normal section of RJ are shown , respectively. Scale bar in (h) is 300 nm for (h) and in (i) is 100 nm.

bending to 10 mm radius, the a-SiGe:H RJ PDs can maintain a superb responsivity of ≈140 mA W^{-1}@800 nm with rise (t_r) and fall (t_f) time scales of 5.4 and 17.6 µs (3.6 µs/13.2 µs before bending). Working at NIR probing light ≈800 nm, rapid pulse signal detection has been successfully demonstrated in PPG reflectance-mode when attached to human wrist, with a configuration as schematically illustrated in Figure 1c, providing a solid basis for developing rapid, comfortable, and high-fidelity sphygmic signal monitoring and diagnostics.

2. Results and Discussion

Figure 1g shows a photograph of the flexible a-SiGe:H RJ@AF units attached to a bent PET substrate, with typical side-view SEM image of the a-SiGe:H RJ units presented in Figure 1h. The standing multilayer RJ junction units are somehow randomly oriented and even mutually crossed, which is a unique aspect of the 3D RJ architecture. To examine the internal RJ structure, enlarged cross section views of broken RJs, roughly in the middle, are displayed in Figure 1i and Figure S3a,b in the Supporting Information, revealing a thin a-SiGe absorber layer with a thickness of only ≈60 nm. A schematic diagram of the as-fabricated radially stacked multilayer structure, with coaxial *p-i-n* junction deposited directly upon the VLS-grown p-type SiNWs, is illustrated in Figure 1j. The SEM images of a single SiNW, a *p-i-n* RJ unit and an ITO-coated *p-i-n* RJ unit are shown in Figure S4a–c in the Supporting Information, respectively. The RJ has an average diameter of ≈300 nm after ITO-coating, which is measured at the middle of RJ, with a height of ≈1000 nm long estimated from the longest RJ found in SEM images. The radially stacked multilayer structure of the RJ units were also examined by using transmission electron microscopy (TEM) characterization and electron diffraction spectroscopy (EDS) analysis for the Si, Ge, In, Sn elements and shown in Figure S4d–k in the Supporting Information, where the center SiNW core, the amorphous (*i*-a-SiGe:H/*n*-a-Si:H) shell layer and the outer ITO layer can be clearly distinguished, with corresponding EDS mapping for the Si, Ge, In and Sn atoms. A band structure diagram of the RJ NIR-PDs is provided in Figure S5a in the Supporting Information, indicating the relative energy levels of the bottom of conduction band E_c, the top of valence band E_v and the Fermi energy level E_f, as well as the photocarriers generation, separation, and collection within the *p-i-n* junction with a-SiGe:H (≈1.4 eV) absorber layer under NIR light illumination.

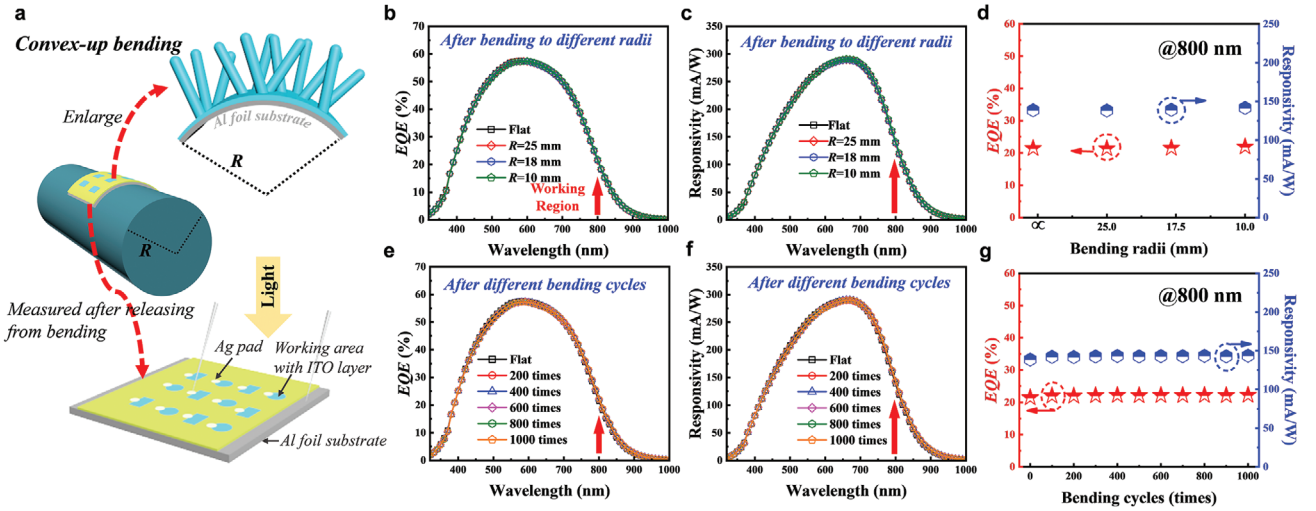

Figure 2. a) Diagram of convex-up bending and testing condition is shown. b) EQE and responsivity curves of the NIR PDs@AF, c) after different bending radii and e,f) after different bending cycles with a small radius of only 10 mm are shown, d,g) extracted values at specific wavelength are shown, respectively.

The flexibility of the RJ NIR-PDs@AF was first tested by attaching them to cylinder rods with different radii, ranging from R = 25 mm to 10 mm, as shown in **Figure 2**a and Figure S5b (Supporting Information), while the optoelectronic properties were measured after bending. No obvious crinkles can be observed on the surface of NIR-PDs@AF even after 1000 times convex-up bending to a very small radius of R = 10 mm (see in Figure S5c in the Supporting Information). The $\text{Responsivity} = \frac{EQE(\%) \times \lambda}{100 \times 1240} \approx 140$ mA W^{-1}@800 nm of the NIR-PDs@AF, deduced from the EQE (≈22%@800 nm) curves in Figure 2b,e according to Ref. [31], remains almost the same even bent to a small radius of only 10 mm for 1000 times, as witnessed in Figure 2c,f. Meanwhile, the extracted values of EQE and responsivity at 800 nm under different bending conditions are shown in Figure 2d,g. The mechanical stability of the RJ NIR-PDs@AF can also be checked by the I–V characteristics measured under NIR light illumination and at ambient conditions after different bending conditions, as presented in Figure S6 in the Supporting Information. Under NIR light illumination (@≈800 nm, ≈30 mW cm^{-2}), the short-circuit current remains almost a constant of ≈79 µA even after 1000 times bending to a small radius of only 10 mm. These results indicate that the NIR-PDs@AF units have excellent flexibility and a rather stable electrical performance under large bending.

Then, the response speeds of the self-powered NIR-PDs@AF devices were characterized with pulsed light signals generated by a NIR LED modulated at 1 kHz, where the light emission was controlled by a signal generator with a center wavelength at ≈800 nm (see in Figure S8a in the Supporting Information). The photovoltages were recorded by oscilloscope in real time, as schematically illustrated in **Figure 3**a. Obviously, the RJ NIR-PDs@AF can well catch up the 1 kHz modulation at NIR wavelength, even bent to a small radius of only 10 mm for 1000 times, as shown in Figure 3b,c. Comparing the enlarged photoresponse curves @1 kHz before and after 1000 times bending, presented in Figure 3d,e respectively, the rise time (t_r) and the fall time (t_f) only change slightly from 3.6 to 5.4 µs or 13.2 to 17.6 µs, respectively. One possible reason for the slower response speed is that the tiny-crack formed among the standing RJ units could lead to a slight decrase of the photocurrent output, causing thus longer charging and discharging response period. Compared to other flexible NIR photodetectors reported in the literature and summarized in Table S1, the self-powered 3D RJ NIR-PDs@AF devices accomplish the fastest responses of 3.6 µs/13.2 µs. This advantage can be assigned to the very thin absorber a-SiGe:H layer (≈60 nm) within the radial junction structures, which enables thus a very efficient and fast separation of the photogenerated carriers within the radial *p-i-n* junction.

To understand the high flexibility of the 3D RJ units, the surfaces of the a-SiGe:H RJ layer forest structure were examined by SEM before and after bending cycles, and shown in **Figure 4**a–c. It is found that the randomly oriented RJ units (Figure 4a) are cross-linked to each other through the touching places at the top, as marked by white dashed circles, which could provide extra conductive top-crossing pathway over the top of the standing RJ forest, in addition to that on the ground surface, as highlighted by the yellow lines in Figure 4a. After 1000 times bending (Figure 4b,c; Figure S9d–f, Supporting Information), cracks emerged on the sample surface but spread only on the ground surface, instead of cutting through the standing RJs. Figure 4c provides an enlarged view of the cracked regions highlighted by green, with typical opening width of ≈160 nm as inferred from the statistics in Figure 4d. Interestingly, the 3D RJs with length of ≈1 µm can still easily touch their neighbor units, over these cracks to keep the continuous top-crossing pathway (marked in Figure 4c and Figure S9a–c (Supporting Information) by yellow lines). Thus, this 3D pathway feature enables a unique capability to overcome the detrimental effect of the cracks, formed for example on the places indicated by the pink rectangles in Figure 4b and Figure S9a–c (Supporting Information). On the other hand, the discrete standing RJ units can also suppress to some extent the unlimited or unidirectional crack spreading,

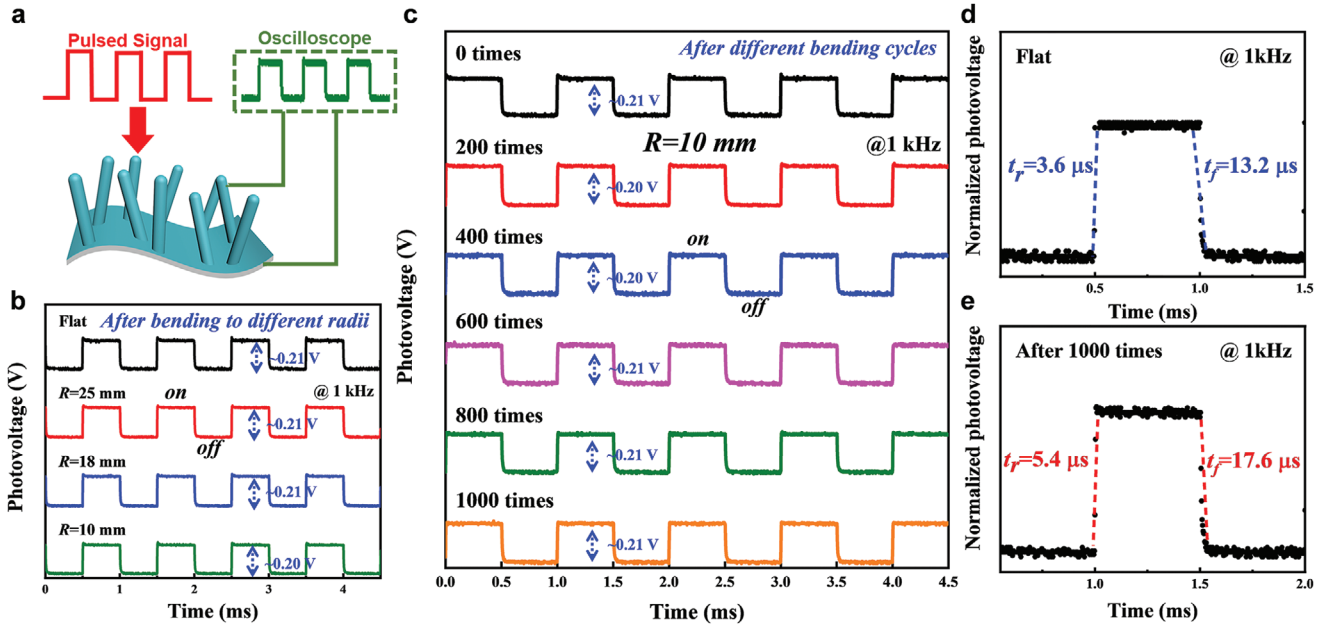

Figure 3. a) Schematic illustration of photo-response speed of the NIR PDs@AF is depicted. b) Time response characteristics of the NIR PDs@AF are shown with different bending radii, and c) after different bending cycles with a small radius of only 10 mm, using NIR LED (@≈800 nm, ≈20 mW cm^{-2}) as light source. d,e) Time response characteristics of the devices without bending and after 1000 times bending @1 kHz are shown, respectively.

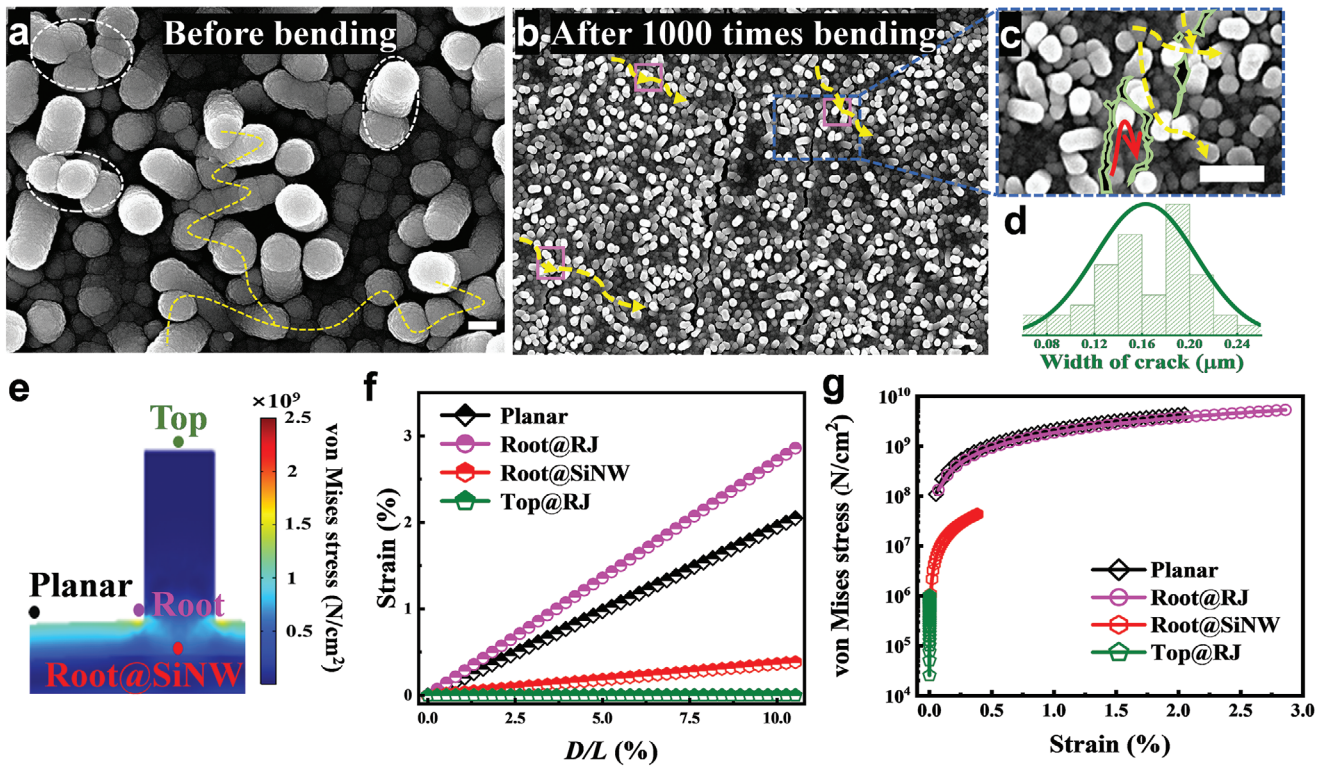

Figure 4. a–c) SEM images before and after bending cycles are shown. d) Statistics of width of cracks induced by 1000 times bending is depicted. e) Simulated von Mises stress distributions along the RJ at four different locations that subjected to convex bending are marked, and the f) evolutions of strains with the value of *D*/*L* is presented. g) Evolutions of stress with different strains are extracted and plotted. Scale bar: 200 nm for (a), 1 μm for (b) and (c).

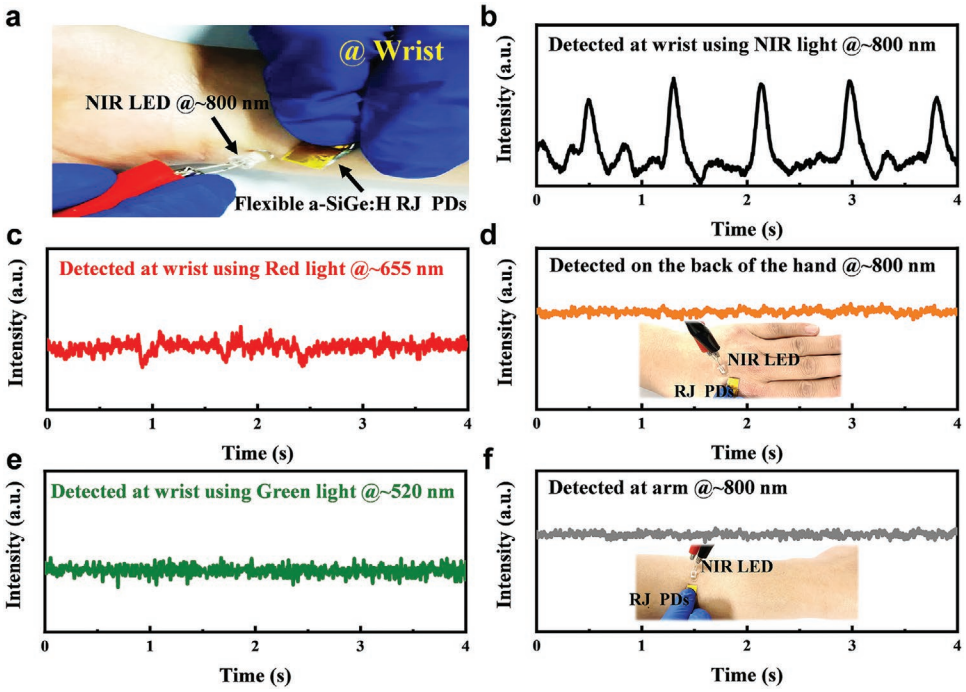

Figure 5. a) Photograph of detecting pulse at wrist is presented. b) Detected pulse signal at wrist is shown. PPG curves at wrist illuminated by c) red light and e) green light are shown, respectively. d,f) The detected curves at vein on the back of the hand, and at arm without any artery, respectively.

preventing the formation of long and continuous cracks and separating the cracks into local and tiny ones as seen Figure 4c and Figure S10a–c (Supporting Information). Finite element simulation of the RJ units standing on flexible AF substrates was also carried out and shown in Figure 4e, where it is shown that, under different bending strain up to 10% on the soft Al surface, the induced strains and the von Mises stresses at the RJ-top (green), RJ-root (purple), planar surface (black) and SiNW-root (red) places are extracted and plotted in Figure 4f,g, respectively. Remarkably, the strains and the stresses felt at the top of the RJs are 3–4 orders of magnitude smaller compared to those found at the roots of RJs and on the nearby planar surface. This indicates that out-of-plane RJ portion hosted by the standing SiNWs can be well protected and separated from the strain-rich and unstable bottom regions. These unique features combined contribute to the excellent flexibility and the mechanical stability of the RJ PDs@AF structure, which is a critical capability for comfortable electronics and allowing for close contact to the soft skin surface.

The flexible a-SiGe:H RJ PDs were then used as PPG biodetector to capture the subdermal pulse signals, by attaching the flexible RJ PDs directly to wrist surface, where the arterial blood volume vibration is more significant and easy to detect,[18] as depicted schematically in Figure S12a in the Supporting Information. Note that, no obvious sphygmic signals were detected at the wrist by using red (**Figure 5**c) and green (Figure 5e) probing light source, due to limited penetration depth into the skin/tissue. Similarly, no discernible PPG signals were detected on the back of hand (Figure 5d) or at arms (Figure 5f) by using a single NIR light source, as in these places the arterial blood volume change associated with heart beating scarcely exists. In comparison, clear and regular PPG signals can be well obtained on the wrist by using single NIR light @≈800 nm, as witnessed in Figure 5b via a NIR-probe-detection configuration depicted in Figure 5a, where the PPG signal is extracted from the variation of NIR light reflected/diffracted from the arterial blood volume vibration, directly caused by the heartbeats. According to the specific PPG signals in Figure 5b, the heart rate was calculated to be 78 ± 5 beats per minute, while the detected PPG signals on different individuals are supplemented in Figure S12b,c in the Supporting Information. These results suggest the flexible a-SiGe:H RJ PDs enable a reliable and convenient single NIR wavelength PPG heart rate detection technology, which can help to chase and extract the heartbeat via solely arterial blood volume change, providing thus a complementary (to the usual oximetry technology) and potentially very useful new dimension for more efficient and accurate diagnostics and real-time health monitoring.

In parallel, heart rate monitoring can also be accomplished based on stretchable electrodes such as silver nanowires and graphene oxide, via pressure/strain-resistance variation sensing.[32–35] Compared to these closely-contacted mechanoelectrical sensing scheme, the flexible a-SiGe:H PDs@AF devices demonstrated here provide a more comfortable and complimentary routine to probe directly the contraction/expansion dynamics of the arterial blood vessels. More importantly, the a-SiGe:H PDs boast a faster response that could enable more advanced real-time PPG analysis.

3. Conclusion

In summary, flexible and robust NIR PDs have been successfully fabricated based on 3D a-SiGe:H radial junction units

constructed over VLS-grown SiNWs grown on thin and soft AF substrates, which enables an efficient detection of NIR with a narrower band-gap of a-SiGe:H alloy thin film. The a-SiGe:H NIR-PDs@AF demonstrate high flexibility and mechanical stability, which can sustain 1000-times bending to very small radius of 10 mm, as well as a responsivity of ≈140 mA W^{-1} at the targeted wavelength @800 nm. Then, the NIR PDs@AF can be well attached to the surface of human wrist for an accurate PPG sphygmic signal detection that relates solely to the arterial blood volume vibration, in contrast to the conventional oximetry technology. This flexible a-SiGe:H RJ technology has a unique potential to enable a new generation of highly flexible photodetectors for rapid, comfortable, and high fidelity sphygmic, as well as other physiological, signal monitoring and diagnostics.

4. Experimental Section

Device Fabrication: The fabrication procedures of the flexible a-SiGe:H RJ NIR photodetectors on 50 µm thick AF substrates (NIR-PDs@AF) were schematically illustrated in Figure 1d–f. First, a 4 nm tin (Sn) layer was thermal evaporated on the surface of AF substrate. Then, it was loaded into the chamber of PECVD and treated by hydrogen (H_2) plasma for 5 min with substrate temperature, flow rate, RF power density and chamber pressure of 200 °C, 20 standard cubic centimeter per minute (SCCM), 10 mW cm^{-2} and 30 Pa, respectively, as shown in Figure 1d, to transform the Sn layer into discrete Sn droplets, which were used to catalyze the VLS-growth of p-type SiNWs. During the VLS process of p-SiNWs, a mixture of 60 SCCM H_2, 6 SCCM silane (SiH_4) and 1.8 SCCM diborane dopant (B_2H_6) precursor gases was introduced, with substrate temperature raised to 350 °C, RF power density and chamber pressure of 20 mW cm^{-2} and 100 Pa, respectively, for 15 min (see Figure 1e). After that, an intrinsic a-SiGe:H alloy layer was deposited around the SiNWs, by a plasma of 20 SCCM H_2, 6 SCCM SiH_4 and 20 SCCM GeH_4 gases (95% H_2-diluted), at 150 °C for 30 min. Then, an n-type doped a-Si:H layer was deposited with 2.6 SCCM phosphine (PH_3) gas for 5 min. Finally, the top ITO layer was deposited through shadow mask by magnetron sputtering, serving as the top transparent electrodes.

Device Characterizations: The morphology of the a-SiGe:H RJ@AF structures was characterized by scanning electron microscopy (SEM, Zeiss Sigma). The nanostructures of a single final-fabricated RJ unit with/without ITO layer and the Energy-dispersive X-ray Spectroscopy (EDS) images were characterized by transmission electron microscopy (TEM) (TecnaiG2F20). The current-voltage (*I–V*) measurements of the a-SiGe:H RJ PDs were conducted under NIR light illumination and at ambient conditions, while the external quantum efficiency (EQE) curves were measured with a calibrated silicon detector by using QEX-10 system within a wavelength range from 320 nm to 1000 nm. The transmittance of pig skin and reflectance of the ITO-coated RJs were characterized by using UV-Vis-NIR Spectrophotometer (UV-3600 Plus, Shimadzu). The response speed was measured using an oscilloscope (InfiniiVision DSOX3052A, KEYSIGHT), and the PDs were illuminated by a pulsed light generated by a waveform generator (Keithley 3390), where the t_r is defined as the rising interval from 10% to 90% of the maximum and the t_f represents the interval required to decrease from 90% to 10%. The PPG signals were characterized by a system consisting of an oscilloscope, a waveform generator, a lock-in amplifier (OE, 1022D DSP), which is schematically illustrated in Figure S12a in the Supporting Information.

Supporting Information

Supporting Information is available from the Wiley Online Library or from the author.

Acknowledgements

The authors acknowledge the financial support from the National Natural Science Foundation of China under Nos. 11874198, 61974064 and 61921005, National Key Research and Development Program of China (2018YFB2200101), and the Fundamental Research Funds for the Central Universities. Informed consent was obtained from the volunteer (the first author) for recording of the PPG signals.

Conflict of Interest

The authors declare no conflict of interest.

Data Availability Statement

Research data are not shared.

Keywords

flexible radial junction photodetectors, Si nanowires, sphygmic signal detection

Received: July 20, 2021
Revised: September 9, 2021
Published online: October 7, 2021

[1] L. Zeng, S. Lin, Z. Lou, H. Yuan, H. Long, Y. Li, W. Lu, S. P. Lau, D. Wu, Y. H. Tsang, *NPG Asia Mater* **2018**, *10*, 352.
[2] C. Xie, B. Nie, L. Zeng, F. Liang, M. Wang, L. Luo, M. Feng, Y. Yu, C. Wu, Y. Wu, S. Yu, *ACS Nano* **2014**, *8*, 4015.
[3] B. Das, N. S. Das, S. Sarkar, B. K. Chatterjee, K. K. Chattopadhyay, *ACS Appl. Mater. Interfaces* **2017**, *9*, 22788.
[4] M. Hossain, G. S. Kumar, S. N. Barimar Prabhava, E. D. Sheerin, D. McCloskey, S. Acharya, K. D. M. Rao, J. J. Boland, *ACS Nano* **2018**, *12*, 4727.
[5] H. Wang, H. Zhen, S. Li, Y. Jing, G. Huang, Y. Mei, W. Lu, *Sci. Adv.* **2016**, *2*, 1600027.
[6] A. Rogalski, *Infrared Phys. Technol.* **2002**, *43*, 187.
[7] L. Tang, S. E. Kocabas, S. Latif, A. K. Okyay, D.-S. Ly-Gagnon, K. C. Saraswat, D. A. B. Miller, *Nat. Photonics* **2008**, *2*, 226.
[8] T. Q. Trung, S. Ramasundaram, B. U. Hwang, N. E. Lee, *Adv. Mater.* **2016**, *28*, 502.
[9] C. M. Lochner, Y. Khan, A. Pierre, A. C. Arias, *Nat. Commun.* **2014**, *5*, 5745.
[10] C. Dagdeviren, Z. Li, Z. L. Wang, *Annu. Rev. Biomed. Eng.* **2017**, *19*, 85.
[11] M. Zhang, J. T. W. Yeow, *Carbon* **2020**, *156*, 339.
[12] Y. Su, X. Wei, F. Peng, Y. Zhong, Y. Lu, S. Su, T. Xu, S. T. Lee, Y. He, *Nano Lett.* **2012**, *12*, 1845.
[13] C. Fuentes-Hernandez, W.-F. Chou, T. M. Khan, L. Diniz, J. Lukens, F. A. Larrain, V. A. Rodriguez-Toro, B. Kippelen, *Science* **2020**, *370*, 698.
[14] L. A. Bortolotto, J. Blacher, T. Kondo, K. Takazawa, M. E. Safar, *Am. J. Hypertens.* **2000**, *13*, 165.
[15] S. Rhee, B.-H. Yang, H. H. Asada, *IEEE Trans. Biomed. Eng.* **2001**, *48*, 795.
[16] J. Y. A. Foo, C. S. Lim, P. Wang, *Physiol. Meas.* **2006**, *27*, 685.
[17] R. Rauh, A. Posfay, M. Muck-Weymann, *Clin. Physiol. Funct. Imaging.* **2003**, *23*, 344.

[18] J. Allen, *Physiol. Meas.* **2007**, *28*, R1.
[19] J. Li, H. Duan, K. Pu, *Adv. Mater.* **2019**, *31*, 1901607.
[20] S. Chen, A. Z. Weitemier, X. Zeng, L. He, X. Wang, Y. Tao, A. J. Y. Huang, Y. Hashimotodani, M. Kano, H. Iwasaki, L. K. Parajuli, S. Okabe, D. B. L. Teh, A. H. All, I. Tsutsui-Kimura, K. F. Tanaka, X. Liu, T. J. McHugh, *Science* **2018**, *359*, 679.
[21] X. Sun, T. Zhang, J. Wang, F. Yang, L. Xu, J. Xu, Y. Shi, K. Chen, P. Roca i Cabarrocas, L. Yu, *Nano Energy* **2018**, *53*, 83.
[22] M. K. Pathirane, H. Hosseinzadeh Khaligh, I. A. Goldthorpe, W. S. Wong, *Sci. Rep.* **2017**, *7*, 8916.
[23] Z. Liu, B. Wen, L. Cao, S. Zhang, Y. Lei, G. Zhao, L. Chen, J. Wang, Y. Shi, J. Xu, X. Pan, L. Yu, *Adv. Healthcare Mater.* **2020**, *9*, 1901342.
[24] X. Xie, X. Zeng, P. Yang, H. Li, J. Li, X. Zhang, Q. Wang, *Nanoscale Res. Lett.* **2012**, *7*, 621.
[25] X. Xie, X. Zeng, P. Yang, H. Li, J. Li, X. Zhang, Q. Wang, *Phys. Status Solidi A* **2013**, *210*, 341.
[26] F. Yang, J. Wang, J. Lu, Z. Yu, L. Yu, J. Xu, Y. Shi, K. Chen, P. Rocai Cabarrocas, *Adv. Opt. Mater.* **2017**, *5*, 1700390.
[27] G. H. Wang, C. Y. Shi, L. Zhao, H. W. Diao, W. J. Wang, *J. Alloys Compd.* **2016**, *658*, 543.
[28] L. W. Veldhuizen, Y. Kuang, R. E. I. Schropp, *Sol. Energy Mater. Sol. Cells* **2016**, *158*, 209.
[29] Q. Shao, Z. Niu, M. Hirtz, L. Jiang, Y. Liu, Z. Wang, X. Chen, *Small* **2014**, *10*, 1466.
[30] R. J. Zambrano, F. A. Rubinelli, J. K. Rath, R. E. I. Schropp, *J. Non-Cryst. Solids* **2002**, *299–302*, 1131.
[31] S. Manna, S. Das, S. P. Mondal, R. Singha, S. K. Ray, *J. Phys. Chem. C* **2012**, *116*, 7126.
[32] K. Fu, J. Zhou, H. Wu, Z. Su, *Nano Energy* **2021**, *88*, 106258.
[33] H. Jia, X. Yang, Q.-Q. Kong, L.-J. Xie, Q.-G. Guo, G. Song, L.-L. Liang, J.-P. Chen, Y. Li, C.-M. Chen, *J. Mater. Chem. A* **2021**, *9*, 1180.
[34] X. Xu, Z. Liu, P. He, J. Yang, *J. Phys. D: Appl. Phys.* **2019**, *52*, 455401.
[35] L. Zhang, H. Li, X. Lai, T. Gao, X. Zeng, *ACS Appl. Mater. Interfaces* **2020**, *12*, 44360.